analytical chemistry

pubs.acs.org/ac Article

Peptide Nucleic Acid-Functionalized Nanochannel Biosensor for the Highly Sensitive Detection of Tumor Exosomal MicroRNA

Ping-Ping Xiao,‖ Qiang-Qiang Wan,‖ Tangbin Liao, Ji-Yuan Tu, Guo-Jun Zhang,* and Zhong-Yue Sun*

Cite This: *Anal. Chem.* 2021, 93, 10966−10973 Read Online

ACCESS | Metrics & More | Article Recommendations | Supporting Information

ABSTRACT: Compared with free miRNAs in blood, miRNAs in exosomes have higher abundance and stability. Therefore, miRNAs in exosomes can be regarded as an ideal tumor marker for early cancer diagnosis. Here, a peptide nucleic acid (PNA)-functionalized nanochannel biosensor for the ultrasensitive and specific detection of tumor exosomal miRNAs is proposed. After PNA was covalently bound to the inner surface of the nanochannels, the detection of tumor exosomal miRNAs was achieved by the charge changes on the surface of nanochannels before and after hybridization (PNA−miRNA). Due to the neutral characteristics of PNA, the efficiency of PNA−miRNA hybridization was improved by significantly reducing the background signal. This biosensor could not only specifically distinguish target miRNA-10b from single-base mismatched miRNA but also achieve a detection limit as low as 75 aM. Moreover, the biosensor was further used to detect exosomal miRNA-10b derived from pancreatic cancer cells and normal pancreatic cells. The results indicate that this biosensor could effectively distinguish pancreatic cancer tumor-derived exosomes from the normal control group, and the detection results show good consistency with those of the quantitative reverse-transcription polymerase chain reaction method. In addition, the biosensor was used to detect exosomal miRNA-10b in clinical plasma samples, and it was found that the content of exosomal miRNA-10b in cancer patients was generally higher than that of healthy individuals, proving that the method is expected to be applied for the early diagnosis of cancer.

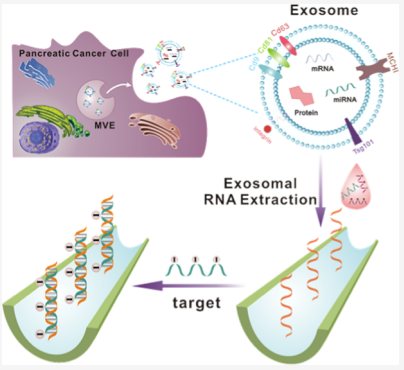

INTRODUCTION

Pancreatic cancer is a common malignant tumor of the digestive tract, accounting for about 1−2% of systemic malignancies.[1] Due to the lack of characteristics of its clinical features and late discovery, it is difficult to make early diagnosis and treatment, which leads to a low survival rate.[2] Therefore, early detection is very important to improve the therapeutic effect of pancreatic cancer. Carbohydrate antigen CA19-9 and carcinoembryonic antigen as conventional markers have been widely used in the diagnosis of pancreatic cancer;[3] although they have high expression in benign diseases and colorectal cancer, the specificity for the early diagnosis of pancreatic cancer is not ideal.[4,5] Therefore, the discovery of specific biomarkers is of great significance for pancreatic cancer diagnosis. Related studies have shown that tumor-derived exosomal miRNAs can be delivered to target cells, thereby directly regulating the gene expression of target cells in the tumor microenvironment.[6−8] Compared with free miRNAs in blood, miRNAs in exosomes are wrapped in lipid membranes to avoid degradation by RNase, so they have higher abundance and stability.[9,10] Moreover, exosomal miRNAs exist in a variety of body fluid environments with a wider sample source. Therefore, exosomal miRNAs are expected to be potential biomarkers for the early diagnosis and prognosis evaluation of cancer.[11,12]

Currently, there are various methods for detecting exosomal miRNAs, such as the gold standard quantitative reverse-transcription polymerase chain reaction (qRT-PCR),[13] electrochemistry,[14−18] fluorescence strategy,[19−21] surface-enhanced Raman scattering,[22,23] and so on.[24] qRT-PCR has a high accuracy for exosomal miRNA detection, but it requires cDNA synthesis and is susceptible to be interfered by other miRNA fragments of exosomes.[25] In comparison, the enzyme-free sensor method has a high sensitivity in exosome miRNA detection. For instance, Liu et al.[26] developed a sandwich electrochemical strategy for exosomal miRNA determination, which could coordinate peptide nucleic acid (PNA) and serinol nucleic acid nanoprobes for the ultrasensitive detection of miRNA-21 derived from tumor exosomes. This system has the ability to distinguish cancer patients from normal individuals in clinical samples. Zhai et al.[21] reported a fluorescence method using gold nanoflare probes (AuNPs) to detect exosomal miRNA-1246 in situ for the breast cancer

Received: May 5, 2021
Accepted: July 23, 2021
Published: July 30, 2021

https://doi.org/10.1021/acs.analchem.1c01898
Anal. Chem. 2021, 93, 10966−10973

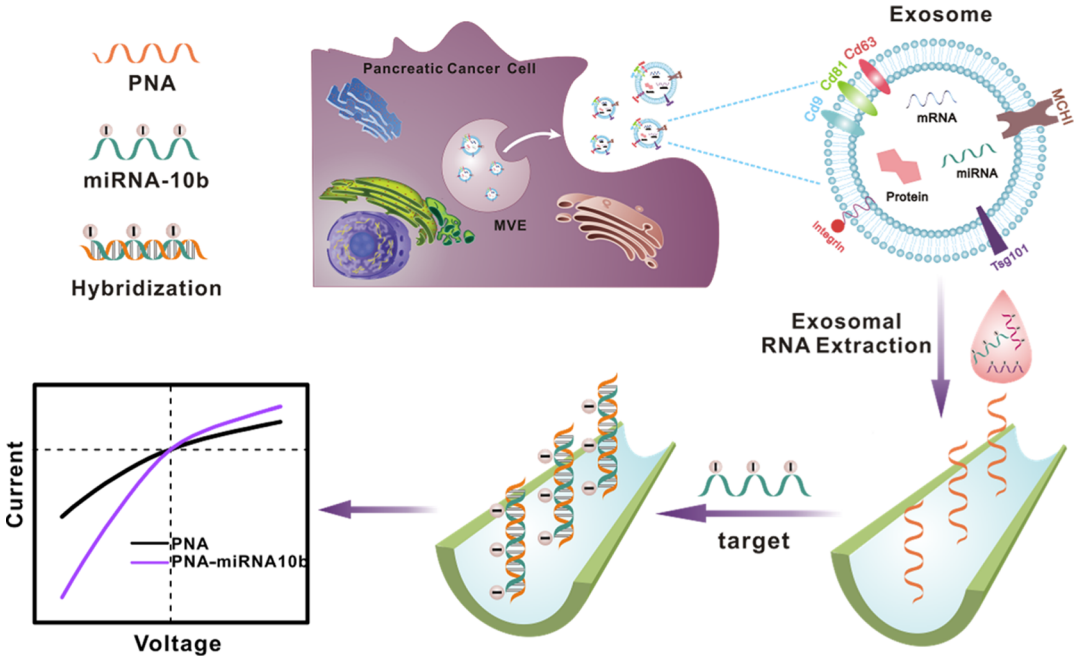

Figure 1. Schematic diagram of exosomal miRNA detection based on the PNA-functionalized nanochannel biosensor.

assay. The synthetic spherical nucleic acid-modified AuNPs could get into the exosomes and hybridize with target miRNA-1246 to generate quantitative fluorescence signals. The above-mentioned methods can achieve the specific detection of exosomal miRNA, but they also have inherent problems, such as time-consuming with multiple hybridization and multiple cleaning processes, interference of background fluorescence signals, and so forth. Therefore, it is particularly necessary to develop a simple and ultrasensitive sensing strategy for the detection of exosomal miRNA.

Until now, nanochannel-based biosensors have been widely developed.[27−33] Their special three-dimensional nanostructure and high specific surface area, as well as controllable channel inner diameter and variety of functional groups, enable them to detect substrates with high specificity, sensitivity, and rapidity.[34−36] For instance, Xia et al.[37] demonstrated a nanochannel sensing device for detecting oligonucleotide DNA and small-molecule adenosine 5′-triphosphate, achieving the highly sensitive detection of DNA by constructing capture probe-DNA-signal probe sandwich nanostructures in nanochannels with a detection limit as low as 10 fM. Liao et al.[38] constructed a phosphorodiamidate morpholino oligos-modified conical nanochannel system to achieve the ultrasensitive detection of free miRNA (Let-7b) in blood. This sensor could distinguish target miRNA from single-base mismatched and noncomplementary sequences, with a low detection limit in the phosphate-buffered saline (PBS) buffer and serum. However, nanochannel sensors have not yet been involved in the detection of exosome-derived miRNAs. Therefore, the design and development of nanochannel-based biosensors for the ultrasensitive and highly specific detection of tumor exosomal miRNAs provide a new strategy for the early diagnosis of cancer.

Herein, we report a PNA-functionalized nanochannel biosensor for tumor exosomal miRNA detection with ultrasensitivity and high specificity. The detection strategy is illustrated in Figure 1. In this system, PNA is chosen as the probe and covalently bound to the nanochannel surface. The neutrality of the PNA greatly reduces the hybridization background signal and eliminates the electrostatic repulsion between the hybridized chains, which improves the hybridization efficiency. Then, we collected exosomes secreted after the starvation culture of pancreatic cancer cells and used the kit to extract total RNA from the collected exosomes. Finally, the target miR-10b in total RNA is detected with our nanochannel sensor.[39] The success of sequence-specific PNA/miRNA duplex formation on the inner walls was monitored via the change in the ionic current. The conductance was positively correlated with the surface charge density of the nanochannels. Compared with the PNA-modified channel, the PNA−miRNA hybridization enhanced the charge density on the channel surface due to the contribution of the negatively charged phosphate backbone of miRNA. The successful capture of exosomal target miRNA was reflected in the increase of ion current. Due to the neutral characteristics of PNA, high specific surface area, and nanoscale confining effect of nanochannels, this biosensor achieves highly sensitive detection of exosomal miRNA without using any signal amplification strategy.

EXPERIMENTAL SECTION

Materials and Reagents. Polyethylene terephthalate (PET) membranes, with 12 μm thickness, were irradiated by a Au ion beam with an energy of 11 MeV/nucleon (ion fluence: 10^7 ions/cm^2, GSI, Germany). The diameter of the etched area is 0.3 cm, so the number of channels in the detection area is about 7×10^5 pores. All miRNAs were synthesized by Sangon Biotech (Shanghai, China). PNA was synthesized by SBS Genetech Co. Ltd. (Beijing, China). Table S1 shows the above-mentioned oligonucleotide sequence. Sodium hydroxide (NaOH), formic acid (HCOOH), and other chemical reagents were obtained from Sinopharm Chemical Reagent Co. Ltd. (Shanghai, China). 1-Ethyl-3-(3-dimethylaminopropyl) carbodiimide (EDC, 98%), RNaseZap, and *N*-hydroxysuccinimide (NHS, 98%) were purchased from Sigma-Aldrich (St. Louis, MO, USA). Bovine serum albumin (BSA) was provided by Wuhan Service biotechnology Co. Ltd.

https://doi.org/10.1021/acs.analchem.1c01898
Anal. Chem. 2021, 93, 10966−10973

(Wuhan, China). PDCA patient-derived cancer cell lines (PANC-1) and healthy pancreatic cells (HPDE6-C7, H6C7) were provided by the American Type Culture Collection (ATCC, Manassas, VA, USA). Exosome Precipitation Solution was provided by System Biosciences (America), and the exoRNeasy Serum/Plasma Midi Kit was provided by Qiagen (Germany). Wuhan First Hospital provided clinical plasma samples. All subjects obtained informed consent. Cienry Biological Technology Co., Ltd. (Zhejiang, China) provided molecular biology-level ultrapure water for preparing solutions.

Preparation of Conical Nanochannels. The conical nanochannels were fabricated through latent ion-asymmetric chemical etching.[40] First, each side of the PET membrane was irradiated with 365 nm ultraviolet light for 1 h. Then, the film was fixed between two tetrafluoroethylene electrolyzers. Under the condition of 35 °C, the acid liquor (1 M KCl + 1 M HCOOH) was filled into one side of the electrolytic cell. After that, the alkali liquor (9 M NaOH) was added on the other side, and double Pt electrodes were used for etching. Keithley's 6487 picoammeter (Keithley Instruments, Cleveland, OH, USA) was used to monitor the ionic current generated through the channels. When the current value reached the required level, the alkali liquor was immediately sucked out. Then, the acid liquor was added to the etching electrolytic cell, sweeping the field for 30 min to neutralize the residual lye in the channel. After that, the film was washed with ultrapure water and soaked overnight. The diameter of the pore size and the cross section of the nanochannels were measured using a field-emission scanning electron microscope. The large opening and the small opening of the nanochannels are about 800 and 34 nm, respectively, and the cross section also shows the typical conical structure (Figure S1).

Immobilization of PNA. When the nanochannels were fabricated, carboxyl groups (−COOH) were observed on the channel surface. 3 mg/mL NHS and 15 mg/mL EDC were prepared in the (N-morpholino) ethanesulfonic acid (MES) buffer (0.1 mol/L, pH 5.4). The membrane was immersed in the above mixed solution for 40 min to activate −COOH into amine-reactive ester molecules.[41] After activation, the membrane was rinsed with the MES buffer. Next, the NHS-ester molecule was covalently condensed to the terminal amine group of the PNA probe (10 μL) at room temperature overnight, and then the PET membrane was rinsed thoroughly. Then, the unreacted active sites were blocked with BSA solution (10 mg/mL, 1 h) to reduce adsorption interference, followed by rinsing thoroughly with ultrapure water. In this system, 0.5× PBS, pH = 7.2 was chosen to monitor the current−voltage (I−V) curves.

PNA−miRNA Hybridization. PNA−miRNA hybridization was performed by dropping the target miRNA solution of appropriate concentration onto both sides of the membrane and incubating for 2 h. After PNA−miRNA hybridization, the film was rinsed with ultrapure water to remove unhybridized miR-10b. The transmembrane ionic current was measured before and after hybridization.

Transmembrane Current Measurement. The nanochannel film was fixed between two tetrafluoroethylene electrolyzers, and both cells were filled with 0.5× PBS (pH 7.2). The Ag/AgCl electrodes were inserted into the chambers of the two tetrafluoroethylene cells, respectively. The current value of each cycle was collected under the scanning voltage from −2 to +2 V, and the measurement cycle was 40 s. The test was repeated five times to get the average value of the I−V curve.

Cell Culture, Exosome Isolation, and Total RNA Extraction. The culture and starvation process of the two types of cells were consistent with those of our previous work.[42] The cell culture medium after starvation was further centrifuged for the isolation of exosomes, and the operational details are described in the Supporting Information. Finally, the ExoQuick-TC Exosome Precipitation Solution was applied to obtain exosomes from the clarified medium. The exoRNeasy Serum/Plasma Midi Kit was chosen to collect plasma exosomes and extract total RNA from cell exosomes and plasma exosomes.

Characterizations. The diameter of nanochannels was measured by field-emission scanning electron microscopy (FE-SEM). Laser scanning confocal microscopy (LSCM) images were measured by a Zeiss confocal laser scan containing the LSM710 module. X-ray photoelectron spectroscopy (XPS) data were obtained by an ESCALAB 250Xi X-ray photoelectron spectroscope (Thermo Fisher, America), and the source gun types were Al and Kα. Nanoparticle tracking analysis (NTA), transmission electron microscopy (TEM), and western blotting analysis were applied to characterize exosomes.

RESULTS AND DISCUSSION

PNA Modification on the Nanochannel Surface. First of all, the chemical etching of nanochannels in the PET membrane produces COOH groups on the channel surface. Under neutral conditions, deprotonated carboxyl groups result in negative charges on the channel surface. Second, the terminal amino group on the PNA probe is covalently coupled to the carboxyl group on the channel surface through a water-soluble EDC and NHS mixture. Subsequently, the unreacted activation sites are blocked with BSA solution. The above process is illustrated in Figure 2A.

The modification of each step of the conical nanochannels was characterized by the corresponding current−voltage curves (Figure 2B). As mentioned above, the surface of the unmodified PET nanochannels is negatively charged. The selective permeation of ions through the nanochannels under

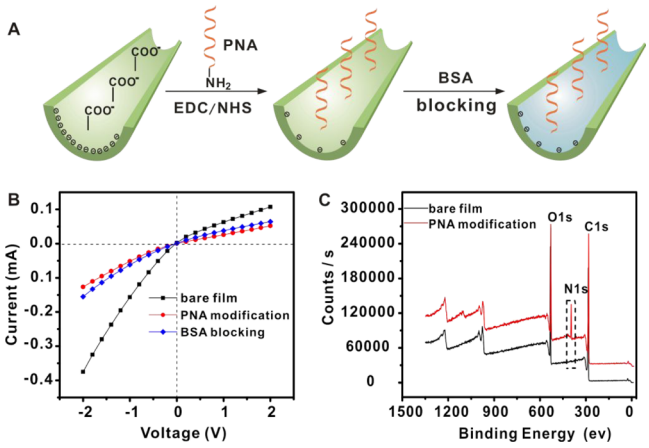

Figure 2. (A) Schematic diagram of the modification process of the PNA-functionalized nanochannels. (B) I−V characteristic curve of the stepwise surface modification process. (C) XPS spectrum of the unmodified nanochannels and the PNA-modified nanochannel surface.

https://doi.org/10.1021/acs.analchem.1c01898
Anal. Chem. 2021, 93, 10966−10973

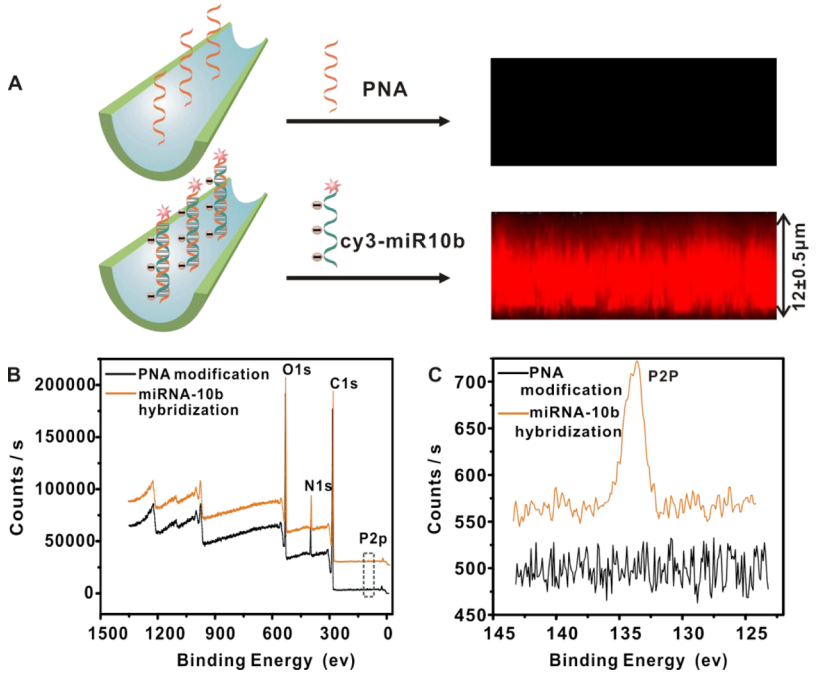

Figure 3. (A) LSCM analysis before and after the hybridization of Cy3-miR-10b with PNA on the inner surface of the channel. (B) XPS spectrum of the PNA-modified nanochannels and the nanochannels after hybridization between PNA and miR-10b. (C) XPS narrow scanning (P2p analysis) of the PNA-modified nanochannels and the nanochannels after hybridization between PNA and miR-10b.

−2 V potential was measured (black line), and the average rectified ion current obtained was −0.375 mA. After modifying the uncharged PNA (red line), the rectified ion current under −2 V reduced from 0.375 to 0.128 mA, corresponding to a decrease of 66%. This is because the neutral PNA probe greatly reduces the negative charge of the channels, resulting in a significant drop in ion rectification. Subsequently, the unreacted activation site was blocked by BSA, and the ion rectification measured at −2 V increased from 0.128 to 0.155 mA, as the negative charge carried by the BSA molecules further increased the negative charge on the channel surface (blue line). Since there are fewer unreacted activation sites, the rectified ion current increases slightly.

In order to further verify the success of modification, XPS was used to evaluate the elemental change of nanochannels before and after PNA probe modification. As shown in Figure 2C, no N 1s peak was observed in the unmodified PET membrane (black line) except for C 1s and O 1s peaks. However, the N 1s peak (red line) appeared after PNA modification. The wettability of the nanochannel before and after PNA modification was measured. The contact angle (CA) values were obtained from the average of five drops at different locations of the membrane. The CA of the etched membrane with unreacted $-COO^-$ was about 57.6° ± 1.8°. After PNA modification, the functionalized surface had a CA of about 43.3° ± 1.2° (Figure S2). The increase in hydrophilicity may be caused by the contribution of the hydrophilic base of PNA. The above results indicate that PNA was successfully fixed on the surface of the nanochannels.

Optimization of Experimental Conditions. The probe concentration and hybridization time of the nanochannel sensor for optimal miRNA detection were investigated (Figure S2). In order to achieve highly orientated spacing and further ordered molecular hybridization at the nanointerface, PNA probe density was first studied. Different PNA concentrations of 5, 10, 15, 20, and 25 μM were employed. When the PNA concentration increased from 5 to 10 μM, the relative ion current change ratio $(I - I_0)/I_0$ (I_0 and I are the current values measured before and after modification, respectively) raised sharply. This was because as the concentration of PNA increased, the carboxyl sites on the channel surface were occupied by a large amount of PNA, resulting in a sharp decrease in the negative charge on the channel surface and therefore a sharp increase in the rate of ion current change. When the PNA concentration increased from 10 to 15, 20, and 25 μM, the current changed slightly, which was because there were fewer unbound carboxyl sites, so the decrease in negative charge was not obvious, and the change in the relative ion current change rate slightly increased. Therefore, the optimal probe concentration was chosen to be 10 μM.

Subsequently, the hybridization time was optimized when the probe concentration was fixed at 10 μM. The PNA-functionalized nanochannels were incubated with 1 nm miR-10b at 1, 1.5, 2, and 2.5 h, respectively. As shown in Figure S3B, the current change ratio $(I - I_0)/I_0$ (I_0 and I are the current values measured before and after hybridization, respectively) increased rapidly from 1 to 2 h. While the hybridization time exceeded 2 h, the current change ratio increased slightly, meaning that the hybridization was saturated. In this work, 2 h was selected as the proper hybridization time. In summary, subsequent experiments were carried out under the above-mentioned optimal conditions.

The ion current of the PNA-modified membrane was measured after 1, 2, 3, 4, 5, 6, and 7 days, respectively. As shown in Figure S4, even after 7 days, the current change ratio $(I - I_0)/I_0$ (I_0 is the current values measured when PNA was modified on the channel surface and I is the current values measured after 1, 2, 3, 4, 5, 6, and 7 days, respectively) of the PNA-functionalized nanochannels also retained about 90%,

https://doi.org/10.1021/acs.analchem.1c01898
Anal. Chem. 2021, 93, 10966−10973

which proved that PNA-modified nanochannels had good stability.

Verification of PNA−miRNA Successful Hybridization. LSCM was used to verify the hybridization of PNA−miRNA on the inner surface of the nanochannels. As shown in Figure 3A, the biosensor immobilized with probe PNA was incubated with 1 nM Cy3-labeled miR-10b at room temperature. There was no fluorescence in the PNA-functionalized channels before hybridization. However, a clear red fluorescent signal appeared in the nanochannels after the interaction of PNA with Cy3-miR-10b, indicating that Cy3-miR-10b had been successfully hybridized with the PNA probe. What is more, the fluorescence characterization proves that the film thickness is equivalent to the physical thickness of the PET film.

XPS analysis was carried to further confirm the success of PNA−miRNA hybridization. The PNA-functionalized nanochannel sensor was incubated with 1 nM miR-10b, and XPS analysis was adopted to detect whether the phosphorus element of miR-10b appeared on the channel surface. The peaks of C 1s, O 1s, and N 1s (Figure 3B) could be clearly observed on the PNA-modified membrane (black line). After PNA was hybridized with miR-10b, the local P2p (135 eV) peak appeared (Figure 3C), indicating that miR-10b had hybridized with the probe PNA. These data indicate that the PNA probe and the target miR-10b were successfully hybridized on the nanochannel surface.

Specificity. The specificity of the sensor to target miR-10b was investigated. The PNA-modified nanochannels were incubated with 1 nm miR-21 (noncomplementary sequence), miR-10a (single-base mismatched sequence), and target miR-10b (complementary), respectively, for 2 h at room temperature. Then, the membrane was rinsed with ultrapure water to wash away unbound miRNA molecules. In this experiment, PBS was used as a blank control. As shown in Figure 4A, after incubating the modified channel with miR-21, the relative ion current change rate hardly changed. When the sensor interacted with miR-10a, similarly, the current change was negligible. When the nanochannel biosensor interacted with miR-10b, the current increased significantly. Figure 4B calculates the relative ionic current change rates before and after hybridization. It can be seen that the relative ion current change of miR-10b is much larger than that of one-base mismatched miR-10a and noncomplementary miR-21, proving that the biosensor has the ability to clearly distinguish miR-10b from single-base mismatched and noncomplementary miRNA. The results show that the biosensor has significant specificity.

Sensitivity. The sensitivity of the nanochannel biosensor was investigated by hybridizing different concentrations of miR-10b with the PNA-modified nanochannels. 0.5×PBS was used as the blank control. It can be seen that the ionic current increased with the increasing concentration of miR-10b (Figure 4C). As shown in Figure 4D, in the wide dynamic range of 100 aM−1 nM, there is a significant linear correlation between the change of the $(I - I_0)/I_0$ signal and the logarithm of the miR-10b concentration ($LgC_{miR\text{-}10b}$), with a correlation coefficient (R^2) of 0.992. The linear regression equation is $(I-I_0)/I_0 = 2.2447 + 0.1336 \times LgC_{miR\text{-}10b}$. The experiment was repeated three times to calculate the error bars. According to the detection limit = $3\sigma/S$ formula, the detection limit was calculated to be 75 aM (σ is the standard deviation of the blank signal; S is the slope of the fitting line). Compared with other exosomal miRNA-sensing methods (Table S2), sensors based on nanochannels can achieve a lower detection limit of 75 aM without employing the signal amplification strategy. That is because the special three-dimensional nanoscale confining characteristics of the nanochannel sensor and neutral characteristics of PNA improve the efficiency of PNA−miRNA hybridization.

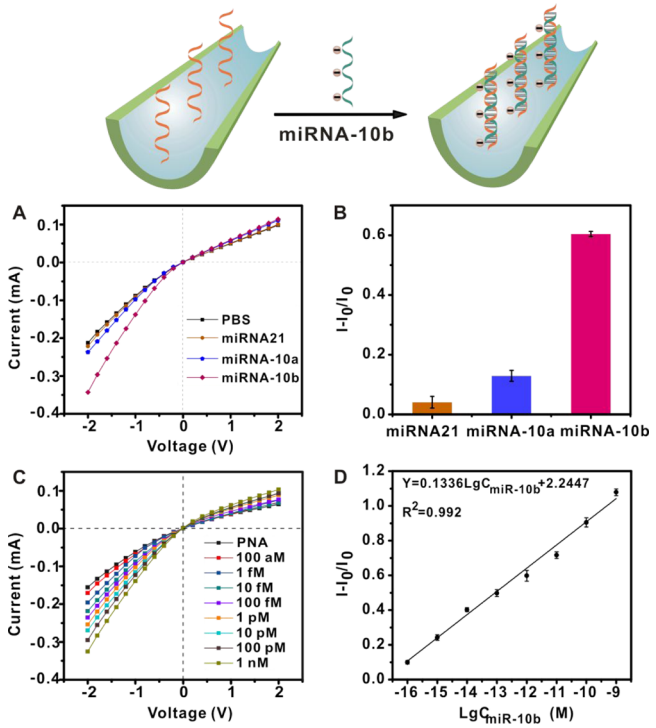

Figure 4. (A) I−V curves of the PNA-functionalized nanochannel biosensor incubated with 1 nM miR-21, miR-10a, and miR-10b, respectively. (B) Ion current change ratios of the modified nanochannels before and after incubating with the three miRNA strands. (C) I−V curves of the nanochannel biosensor incubated with a range of miR-10b concentrations. (D) Linear relationship between the ion current change rate and the concentration of miR-10b.

Exosomal miRNA Detection. MicroRNAs are the key components of exosomes. Tumor microRNAs delivered by exosomes participate in tumor progression by regulating the microenvironment, angiogenesis, immune evasion, and metastasis, which are of great significance for early cancer diagnosis. Exosomes were collected from the PANC -1 and H6C7 culture medium, and total RNA was extracted for miR-10b detection. First, the collected exosomes were purified and their morphology was observed by TEM. Figure 5A shows that the purified exosomes had a double-membrane circular structure, which was in accordance with previous reports.[42,43] The magnified TEM image reflects the typical cup-shaped exosome morphology (inset). Next, NTA analysis shows that the size distribution of the collected exosomes derived from PANC-1 was located at 120 nm (Figure 5B) and an initial concentration of 1.2×10^{11} particles/mL was obtained (Figure S3B). Similar characterization results of H6C7-derived exosomes are shown in Figure S3A,C−D. Western blotting analysis further verifies the successful extraction of exosomes. As shown in Figure 5C, the conventional protein markers CD63, GPC-1, and EpCAM bands of exosomes could be clearly observed, which proved the successful extraction of exosomes from PANC-1 and H6C7. Subsequently, the total RNA extracted from PANC-1- and H6C7-derived exosomes, respectively, interacted with the PNA-functionalized nano-

https://doi.org/10.1021/acs.analchem.1c01898
Anal. Chem. 2021, 93, 10966−10973

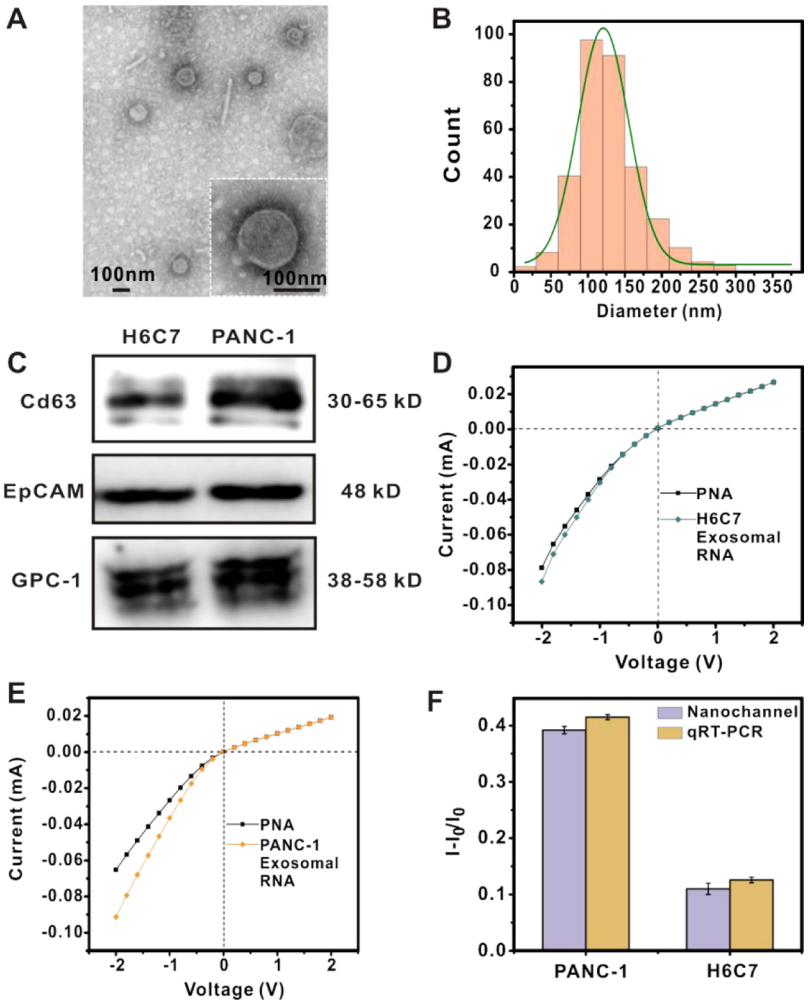

Figure 5. (A) TEM image of PANC-1 exosomes. The inset shows an enlarged, typical cup-shaped exosomal structure. Scale bars: 100 nm. (B) Size distribution of the collected PANC-1 exosomes. (C) WB shows the expression of CD63, EpCAM, and GPC-1 in exosomes from PANC-1 and H6C7 cell lines, respectively. (D) I−V curves of the target miR-10b detection in the total RNA extracted from PANC-1- and (E) H6C7-derived exosomes, respectively. (F) Comparison of miRA-10b expression levels in the total exosomal RNA isolated from PANC-1 and H6C7 using qRT-PCR and the nanochannel sensor. The error bars represent the standard errors (n = 3).

channel sensor (Figure 5D,E). Under the same exosome concentration, when the sensor interacted with the total RNA extracted from H6C7-derived exosomes, the ion current change was negligible. The current increased significantly when the sensor was incubated with the total RNA extracted from PANC-1-derived exosomes. The current change ratio of the PANC-1 group was higher than that of the H6C7 group, and the *t*-test proved that the difference between the two groups was significant ($P < 0.001$) (Figure 5F). The results show that the sensor is able to effectively distinguish pancreatic cancer from normal control groups by detecting the tumor-derived exosomal miRNA because the expression level of miR-10b in pancreatic cancer cells is higher than that of normal individuals. To verify the accuracy of our proposed method, qRT-RCR was further used to quantify the exosomal miR-10b level of the two types of cell lines. Comparing the miR-10b level of the nanochannel sensor data with that of qRT-PCR data, it is found that the results are relatively consistent, showing the reliability of the PNA-functionalized nanochannel biosensor (Figure 5F).

Exosomal microRNA Detection in Clinical Blood Samples. To demonstrate the applicability of the PNA-functionalized nanochannel sensor in clinical samples, we investigated its response to miR-10b in the total RNA of exosomes in clinical plasma samples. 20 clinical plasma samples (10 healthy volunteers and 10 pancreatic cancer patients) were collected from Wuhan First hospital. A exoRNeasy Serum/Plasma Midi Kit was used to extract total exosomal RNA, after which miR-10b was analyzed from the total RNA by the PNA-functionalized nanochannel sensing platform. Compared with the signal value of healthy individual samples, it was found that the average current signal of pancreatic cancer patient samples was significantly stronger than that of each healthy sample (Figure 6A). After statistical analysis, there is a significant difference between pancreatic cancer samples and healthy individuals in the expression of plasma exosomal miR-10b ($P < 0.001$) (Figure 6B), which is consistent with the up-regulation of miR-10b in pancreatic cancer patients, as previously reported.[23] The results indicate that the developed sensor is capable of detecting exosomal miRNA in clinical plasma samples and can effectively distinguish plasma samples from cancer patients and healthy people. Heat map analysis shows that there are obvious differences in the expression of miR-10b between pancreatic cancer patients and healthy volunteers

https://doi.org/10.1021/acs.analchem.1c01898
Anal. Chem. 2021, 93, 10966−10973

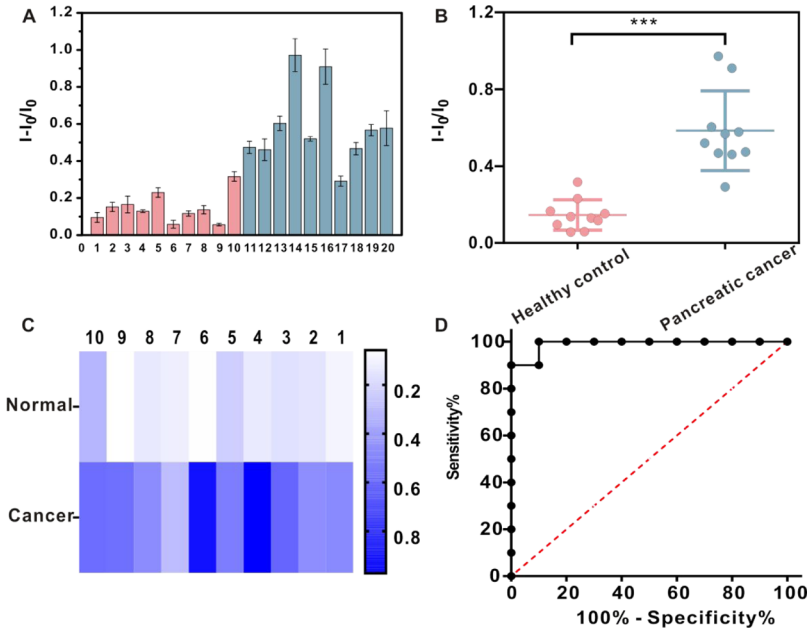

Figure 6. (A) Sensor signals of exosomal miR-10b in plasma samples from 10 healthy volunteers and 10 pancreatic cancer patients. (B) Difference of plasma exosomal miR-10b expression between pancreatic cancer patients and healthy volunteers. (C) Heat map analysis of the plasma exosomal miR-10b level in two groups. (D) ROC curve analysis shows the sensor's ability to discriminate pancreatic cancer patients from the healthy volunteers by comparison of the exosomal miR-10b expression level.

(Figure 6C). The receiver operating characteristic (ROC) curve analysis was performed on the detection results of the sensor on 20 clinical plasma samples to further evaluate the detection performance of the nanochannel sensor (Figure 6D). The abscissa of the ROC curve has 100% specificity, and the ordinate is sensitive. The calculated area under the curve of this method is 0.99 and $P < 0.001$. The analysis of clinical samples not only verifies that exosomal miR-10b is a promising biomarker for the early diagnosis of pancreatic cancer but also shows that the PNA-functionalized nanochannel biosensor we constructed provides a novel idea and platform for exosomal miRNA detection, which is meaningful for clinical analysis.

CONCLUSIONS

In summary, the PNA-functionalized nanochannel sensing platform has been developed and it has been used to detect exosomal miR-10b derived from pancreatic cancer in a sensitive and specific manner. Because of the neutral characteristics of PNA and the merits of nanochannels, a high detection sensitivity is achieved. Moreover, the sensor shows high specificity and it can effectively distinguish pancreatic cancer tumor-derived exosomes from the normal control group. The detection results are in good consistency with those obtained by the qRT-PCR method. In addition, clinical plasma samples are analyzed by the PNA-functionalized nanochannel sensor, and the results prove that the contents of exosomal miRNA-10b in pancreatic cancer patients are generally higher than those of healthy persons. This indicates that this sensor can differentiate exosomal miRNA expression in the plasma of cancer patients and healthy people, showing clinical application potential in the early diagnosis of cancer.

ASSOCIATED CONTENT

Supporting Information

The Supporting Information is available free of charge at https://pubs.acs.org/doi/10.1021/acs.analchem.1c01898.

Characterization of exosomes, qRT-PCR protocol, PNA probe sequence and miRNA sequences, comparison of different methods for exosomal miRNA detection, FE-SEM images of conical PET nanochannels, wettability of nanochannel before and after PNA modification, optimizations of experimental conditions, stability of the PNA-functionalized nanochannel biosensor, and TEM characterizations and NTA results of H6C7 exosomes (PDF)

AUTHOR INFORMATION

Corresponding Authors

Guo-Jun Zhang − *School of Laboratory Medicine, Hubei University of Chinese Medicine, Wuhan 430065, China*; Email: shui10123@aliyun.com

Zhong-Yue Sun − *School of Laboratory Medicine, Hubei University of Chinese Medicine, Wuhan 430065, China*; orcid.org/0000-0001-9032-5607; Email: zhanggj@hbtcm.edu.cn

Authors

Ping-Ping Xiao − *School of Laboratory Medicine, Hubei University of Chinese Medicine, Wuhan 430065, China*

Qiang-Qiang Wan − *School of Laboratory Medicine, Hubei University of Chinese Medicine, Wuhan 430065, China; Wuhan First Hospital, Wuhan 430022, China*

Tangbin Liao − *School of Pharmacy, Hubei University of Chinese Medicine, Wuhan 430065, China*

Ji-Yuan Tu − *School of Laboratory Medicine, Hubei University of Chinese Medicine, Wuhan 430065, China*

Complete contact information is available at:

https://doi.org/10.1021/acs.analchem.1c01898
Anal. Chem. 2021, 93, 10966−10973

https://pubs.acs.org/10.1021/acs.analchem.1c01898

Author Contributions

[‖]P.P.X. and Q.Q.W. contributed equally.

Notes

The authors declare no competing financial interest.

■ ACKNOWLEDGMENTS

This work was supported by the National Natural Science Foundation of China (21974035) and Health Commission of Hubei Province (WJ2021M213).

■ REFERENCES

(1) Kleeff, J.; Ishiwata, T.; Kumbasar, A.; Friess, H.; Büchler, M. W.; Lander, A. D.; Korc, M. *J. Clin. Invest.* **1998**, *102*, 1662−1673.
(2) Hidalgo, M. *Rev. Infirm. Assist. Soc.* **2010**, *362*, 1605−1617.
(3) Kim, J.; Bamlet, W. R.; Oberg, A. L.; Chaffee, K. G.; Donahue, G.; Cao, X.-J.; Chari, S.; Garcia, B. A.; Petersen, G. M.; Zaret, K. S. *Sci. Transl. Med.* **2017**, *9*, No. eaah5583.
(4) Goonetilleke, K. S.; Siriwardena, A. K. *Eur. J. Surg. Oncol.* **2007**, *33*, 266−270.
(5) Datta, J.; Vollmer, C. M. *South. Med. J.* **2014**, *107*, 256−263.
(6) Azmi, A. S.; Bao, B.; Sarkar, F. H. *Cancer Metastasis Rev.* **2013**, *32*, 623−642.
(7) Yang, M.; Chen, J.; Su, F.; Yu, B.; Su, F.; Lin, L.; Liu, Y.; Huang, J.; Song, E. *Mol. Cancer* **2011**, *10*, 117.
(8) Li, L.; Li, C.; Wang, S.; Wang, Z.; Jiang, J.; Wang, W.; Li, X.; Chen, J.; Liu, K.; Li, C.; Zhu, G. *Cancer Res.* **2016**, *76*, 1770−1780.
(9) Cheng, L.; Sharples, R. A.; Scicluna, B. J.; Hill, A. F. *J. Extracell. Vesicles* **2014**, *3*, 23743.
(10) Sanz-Rubio, D.; Martin-Burriel, I.; Gil, A.; Cubero, P.; Forner, M.; Khalyfa, A.; Marin, J. M. *Sci. Rep.* **2018**, *8*, 10306.
(11) Guo, Z.; Zhao, C.; Wang, Z. *Tumour Biol.* **2014**, *35*, 10395−10407.
(12) Zhang, Y.; Sui, J.; Shen, X.; Li, C.; Yao, W.; Hong, W.; Peng, H.; Pu, Y.; Yin, L.; Liang, G. *Oncol. Rep.* **2017**, *37*, 3543−3553.
(13) Chen, C.; Ridzon, D. A.; Broomer, A. J.; Zhou, Z.; Lee, D. H.; Nguyen, J. T.; Barbisin, M.; Xu, N. L.; Mahuvakar, V. R.; Andersen, M. R.; Lao, K. Q.; Livak, K. J.; Guegler, K. J. *Nucleic Acids Res.* **2005**, *33*, No. e179.
(14) Guo, Q.; Yu, Y.; Zhang, H.; Cai, C.; Shen, Q. *Anal. Chem.* **2020**, *92*, 5302−5310.
(15) Ghazizadeh, E.; Naseri, Z.; Jaafari, M. R.; Forozandeh-Moghadam, M.; Hosseinkhani, S. *Biosens. Bioelectron.* **2018**, *113*, 74−81.
(16) Liu, P.; Qian, X.; Li, X.; Fan, L.; Li, X.; Cui, D.; Yan, Y. *ACS Appl. Mater. Interfaces* **2020**, *12*, 45648−45656.
(17) Miao, P.; Tang, Y. *Anal. Chem.* **2020**, *92*, 12026−12032.
(18) Liu, N.; Lu, H.; Liu, L.; Ni, W.; Yao, Q.; Zhang, G. J.; Yang, F. *Anal. Chem.* **2021**, *93*, 5917−5923.
(19) Lee, J. H.; Choi, J. H.; Chueng, S. D.; Pongkulapa, T.; Yang, L.; Cho, H. Y.; Choi, J. W.; Lee, K. B. *ACS Nano* **2019**, *13*, 8793−8803.
(20) Zhao, J.; Liu, C.; Li, Y.; Ma, Y.; Deng, J.; Li, L.; Sun, J. *J. Am. Chem. Soc.* **2020**, *142*, 4996−5001.
(21) Zhai, L.; Li, M.; Pan, W.; Chen, Y.; Li, M.; Pang, J.; Zheng, L.; Chen, J.; Duan, W. *ACS Appl. Mater. Interfaces* **2018**, *10*, 39478−39486.
(22) Lee, J. U.; Kim, W. H.; Lee, H. S.; Park, K. H.; Sim, S. J. *Small* **2019**, *15*, No. e1804968.
(23) Pang, Y.; Wang, C.; Lu, L.; Wang, C.; Sun, Z.; Xiao, R. *Biosens. Bioelectron.* **2019**, *130*, 204−213.
(24) Joshi, G. K.; Deitz-Mcelyea, S.; Liyanage, T.; Lawrence, K.; Mali, S.; Sardar, R.; Korc, M. *ACS Nano* **2015**, *9*, 11075−11089.
(25) Chevillet, J. R.; Kang, Q.; Ruf, I. K.; Briggs, H. A.; Vojtech, L. N.; Hughes, S. M.; Cheng, H. H.; Arroyo, J. D.; Meredith, E. K.; Gallichotte, E. N.; Pogosova-Agadjanyan, E. L.; Morrissey, C.; Stirewalt, D. L.; Hladik, F.; Yu, E. Y.; Higano, C. S.; Tewari, M. *Proc. Natl. Acad. Sci. U.S.A.* **2014**, *111*, 14888−14893.
(26) Liu, L.; Lu, H.; Shi, R.; Peng, X. X.; Xiang, Q.; Wang, B.; Wan, Q. Q.; Sun, Y.; Yang, F.; Zhang, G. J. *Anal. Chem.* **2019**, *91*, 13198−13205.
(27) Zhu, L.; Miao, M.; Shao, X.; Du, Z.; Huang, K.; Luo, Y.; Xu, W. *Anal. Chem.* **2019**, *91*, 14992−14999.
(28) Li, M.; Xiong, Y.; Lu, W.; Wang, X.; Liu, Y.; Na, B.; Qin, H.; Tang, M.; Qin, H.; Ye, M.; Liang, X.; Qing, G. *J. Am. Chem. Soc.* **2020**, *142*, 16324−16333.
(29) Sun, Z.; Liao, T.; Zhang, Y.; Shu, J.; Zhang, H.; Zhang, G. J. *Biosens. Bioelectron.* **2016**, *86*, 194−201.
(30) Gao, L.; Li, P.; Zhang, Y.; Xiao, K.; Ma, J.; Xie, G.; Hou, G.; Zhang, Z.; Wen, L.; Jiang, L. *Small* **2015**, *11*, 543−547.
(31) Sun, Y.; Chen, S.; Chen, X.; Xu, Y.; Zhang, S.; Ouyang, Q.; Yang, G.; Li, H. *Nat. Commun.* **2019**, *10*, 1323.
(32) Guo, W.; Hong, F.; Liu, N.; Huang, J.; Wang, B.; Duan, R.; Lou, X.; Xia, F. *Adv. Mater.* **2015**, *27*, 2090−2095.
(33) Lou, X.; Song, Y.; Liu, R.; Cheng, Y.; Dai, J.; Chen, Q.; Gao, P.; Zhao, Z.; Xia, F. *Small Methods* **2019**, *4*, 1900432.
(34) Seifert, A.; Göpfrich, K.; Burns, J. R.; Fertig, N.; Keyser, F. U.; Howorka, S. *ACS Nano* **2015**, *9*, 1117−1126.
(35) Kim, B. Y.; Sohn, I. Y.; Lee, D.; Han, G. S.; Lee, W. I.; Jung, H. S.; Lee, N. E. *Nanoscale* **2015**, *7*, 9844−9851.
(36) Ali, M.; Ahmed, I.; Ramirez, P.; Nasir, S.; Niemeyer, C. M.; Mafe, S.; Ensinger, W. *Small* **2016**, *12*, 2014−2021.
(37) Liu, N.; Jiang, Y.; Zhou, Y.; Xia, F.; Guo, W.; Jiang, L. *Angew. Chem.* **2013**, *52*, 2007−2011.
(38) Liao, T.; Li, X.; Tong, Q.; Zou, K.; Zhang, H.; Tang, L.; Sun, Z.; Zhang, G. J. *Anal. Chem.* **2017**, *89*, 5511−5518.
(39) Nakata, K.; Ohuchida, K.; Mizumoto, K.; Kayashima, T.; Ikenaga, N.; Sakai, H.; Lin, C.; Fujita, H.; Otsuka, T.; Aishima, S.; Nagai, E.; Oda, Y.; Tanaka, M. *Surgery* **2011**, *150*, 916−922.
(40) Guo, Z.; Wang, J.; Ren, J.; Wang, E. *Nanoscale* **2011**, *3*, 3767−3773.
(41) Ali, M.; Neumann, R.; Ensinger, W. *ACS Nano* **2010**, *4*, 7267−7274.
(42) Jin, D.; Yang, F.; Zhang, Y. L.; Liu, L.; Zhou, Y.; Wang, F.; Zhang, G. J. *Anal. Chem.* **2018**, *90*, 14402−14411.
(43) Wang, C.; Jin, D.; Yu, Y.; Tang, L.; Sun, Y.; Sun, Z.; Zhang, G.-J. *Sens. Actuators, B* **2020**, *314*, 128056.

https://doi.org/10.1021/acs.analchem.1c01898
Anal. Chem. 2021, 93, 10966−10973